Obrabotka metallov (tekhnologiya, oborudovanie, instrumenty) = Metal Working and Material Science. 2026 vol. 28 no. 2 pp. 196–222
ISSN: 1994-6309 (print) / 2541-819X (online)
DOI: 10.17212/1994-6309-2026-28.2-196-222

NSTU NETI

Obrabotka metallov -
Metal Working and Material Science

Journal homepage: http://journals.nstu.ru/obrabotka_metallov

Investigation of the characteristics of chip formation and wear of working surfaces of milling inserts with CVD coating in high-speed α-Ti machining

Petr Pivkin [1, a], ***Artem Babaev*** [2, b, *], ***Nikolai Savchenko*** [3, c], ***Viktor Kozlov*** [3, d], ***Artem Semenov*** [3, e], ***Vladimir Grechishnikov*** [1, f], ***Ludmila Uvarova*** [1, g] ***Alexey Nadykto*** [1, h]

[1] Moscow State University of Technology "STANKIN", 3a Vadkovski Lane, Moscow, 127055, Russian Federation
[2] National Research Tomsk Polytechnic University, 30 Lenin Avenue, Tomsk, 634050, Russian Federation
[3] National Research Tomsk State University, 36 Lenin Avenue, Tomsk, 634050, Russian Federation, 634050, Russian Federation

[a] https://orcid.org/0000-0002-7547-4652, pmpivkin@gmail.com; [b] https://orcid.org/0000-0003-2334-1679, temkams@mail.ru;
[c] https://orcid.org/0000-0001-8254-5853, savnick@ispms.ru; [d] https://orcid.org/0000-0001-9351-5713, kozlov-victor@bk.ru;
[e] https://orcid.org/0000-0002-8663-4877, artems2102@yandex.ru; [f] https://orcid.org/0009-0001-5535-0724, grechishnikov1935@gmail.com;
[g] https://orcid.org/0000-0003-1137-6436, l.uvarova@stankin.ru; [h] https://orcid.org/0000-0003-3652-7421, abnadykto@yandex.ru

ARTICLE INFO

Article history:
Received: 04 April 2026
Revised: 14 April 2026
Accepted: 30 April 2026
Available online: 15 June 2026

Keywords:
Titanium alloy
High-speed milling
Chip
Wear and tear

Funding
The research carried out with the financial support of the Russian Federation under project No. 22-79-10353-П.

Acknowledgements
The authors express their gratitude to the Center for Collective Use of Physical-Chemical Mathematics (*TPU*).

ABSTRACT

Introduction. Due to the wide application of pure **α**-titanium in critical products, the intensification of its machining by cutting is an urgent task. Existing studies focus mainly on alloyed alloys, while the features of high-speed dry milling of pure **α**-*Ti* are not well understood. ***The aim of this work*** was to investigate the influence of milling modes on the wear of a *CVD*-coating (Al_2O_3/*TiCN+TiN*) on carbide inserts, chip morphology and deformation processes in the surface layer of *Ti Grade 2* alloy. **Methodology**. The experiments were carried out using parallel milling in the range of cutting speeds $\boldsymbol{v}$ = 100–300 m/min, feed rates $\boldsymbol{f}$ = 50–100 mm/min and depths of cut a_p = 0.2–0.4 mm without coolant. The condition of the cutting edges and the morphology of the chips were investigated using *SEM* and *EDX*. X-ray diffraction analysis was used to assess deformation changes. The data were processed using correlation and regression analysis methods. **Results and discussion**. It has been found that with increasing cutting speed, adhesion processes and thermomechanical stresses are intensified, leading to local scraping and delamination of the *CVD* coating on the rake surface. At a speed of 300 m/min, there is significant material buildup, forming an unstable built-up edge. The study of the chips revealed a transition from continuous to elemental form. A strong negative correlation ($\boldsymbol{r}$ = −0.81) between the cutting speed and the height of protrusions ($\boldsymbol{h}_3$) on the chip was found, as well as a moderate positive influence of the depth of cut on the continuity coefficient ($\boldsymbol{r}$ = 0.55). The results obtained are relevant for the optimization of high-speed dry machining of pure titanium products used in cryogenic engineering and heat exchangers. **Conclusions**. The dominant wear mechanisms are adhesion and thermomechanical degradation of the coating. The critical mode leading to intensive buildup is a combination of $\boldsymbol{v}$ = 300 m/min, $\boldsymbol{f}$ = 100 mm/min, a_p = 0.4 mm. To reduce wear, it is recommended to control heat dissipation by optimizing cutting speed and depth of cut.

For citation: Pivkin P.M., Babaev A.S., Savchenko N.L., Kozlov V.N., Semenov A.R., Grechishinikov V.A., Uvarova L.A., Nadykto A.B. Investigation of the characteristics of chip formation and wear of working surfaces of milling inserts with CVD coating in high-speed α-Ti machining. *Obrabotka metallov (tekhnologiya, oborudovanie, instrumenty) = Metal Working and Material Science*, 2026, vol. 28, no. 2, pp. 196–222. DOI: 10.17212/1994-6309-2026-28.2-196-222. (In Russian).

*** Corresponding author**
Babaev Artem S., Ph.D. (Engineering), Senior Researcher
National Research Tomsk State University,
36 Lenin Avenue,
634050, Tomsk, Russian Federation
Tel.: +7 952 805-09-26, **e-mail:** temkams@mail.ru

Introduction

Titanium alloys are widely used in various industries such as aerospace and automotive due to their sufficient strength. Titanium alloys are also used in petrochemical, architectural and various medical devices. This is due to their high specific strength and chemical stability. However, some properties of the alloy cause difficulties in machining. Titanium machining is difficult due to its poor thermal conductivity, high temperature stresses and high compressive loads formed on the working surfaces of the cutting wedge, leading to tool wear and destruction. Even greater difficulties arise with the intensification of machining, i.e. through the use of high cutting speeds, which is justified if it is necessary to accelerate the production of products. An increase in the cutting speed is accompanied by an increase in the machining temperature, which contributes to the softening of the tool material, thereby reducing its service life.

It is known that titanium has polymorphism and exists in two allotropic modifications — a low-temperature modification of **α**-titanium and a high-temperature modification of **β**-titanium. The low-temperature modification takes place at temperatures up to 882.5 °C and is characterised by a hexagonal lattice with close-packed atoms. The high-temperature modification exists at temperatures above 882.5 °C and has a body-centred cubic lattice. Thus, the *Ti Grade 2* alloy studied in this work belongs to **α**-titanium alloys and is characterised by the preservation of plastic properties after prolonged combined exposure to high temperatures and stresses.

The difficulties of machining titanium alloys are described in the work of *R. Komanduri* [1]. The main difficulties include the short tool life and low metal removal rate, which are mainly due to poor thermal properties of the alloy (low thermal conductivity), periodic coarse inhomogeneous deformation, instability of the chip formation process, fluctuations in the components of the cutting force, high temperature in the area of tool–chip contact, high chemical reactivity of the alloy and low modulus of elasticity. The latter causes a large elastic deformation of a part of the metal (the thickness of the layer) extending under the cutting edge of the tool, which subsequently causes a large amount of elastic recovery of the cutting surface in contact with the flank surface of the tool, and, as a result, a large value of normal contact stresses on the flank surface and especially on the wear chamfer on the back surface of the tool [2].

For example, when turning titanium alloys, it is recommended to use a carbide tool (*WC+Co* group) at cutting speeds of less than 60 m/min, which greatly limits the possibilities for accelerating the production of finished products.

To achieve higher machining efficiency, it is necessary to reduce the cutting temperature as much as possible and quickly remove heat from the machining area. According to this principle, it is desirable to use a tool with high thermal conductivity and a large rake angle to reduce heat generation, but high contact stresses on the rake surface of the tool when machining difficult-to-machine groups of titanium alloys force the use of negative rake angles $\boldsymbol{\gamma}$ to minus 30° [3], as well as the use of abundant supply of water-based coolant or other cooling methods [4–6].

On the other hand, the use of coolant is undesirable due to the contamination of expensive titanium chips and the impossibility of further processing [7].

According to research data [8–14], high-speed cutting for titanium alloys is considered to be a mode in which the cutting speed exceeds the range of 150–200 m/min at various feeds and cutting depths. This statement is true for easy-to-machine groups of titanium alloys and technically pure titanium, and for difficult-to-machine groups of titanium alloys, the cutting speed $\boldsymbol{v}$ should not exceed 30 m/min [7].

A review of the literature shows that high-speed milling of titanium alloys is mainly considered in the context of machining alloyed alloys, for example, *Ti-6Al-4V* [15–17].

Thus, in [18], researchers *Jawaid*, *Sharif*, & *Koksal* used carbide tools with *PVD-TiN* and *CVD-TiCN/*Al_2O_3 coatings for face milling of *Ti-6Al-4V* alloy with different cutting speeds: 55, 65, 80, and 100 m/min, with a feed rate of 0.1 and 0.15 mm per tooth, axial cutting depth of 2 mm and radial cutting depth of 58 mm. The cutting efficiency was evaluated in terms of wear mechanisms, tool durability, and types of failures. The authors noted excessive chipping and plastic deformation of the cutting edge, peeling and/or chipping of the rake surface, as well as uneven wear of the flank surface, which is the dominant sign of wear on both *PVD*- and *CVD*-coated tools.

In [19], the machinability of *Ti-6.5Al-2Zr-1Mo-1V* alloy during high-speed milling was studied in terms of tool wear and surface integrity. The wear of cutting tools with the formation of a groove (furrow) increases with increasing cutting speed, which leads to a decrease in the cutting tool life. With high-speed milling, it was possible to achieve good surface integrity of the workpiece.

In the study [20], the authors conducted experiments on dry milling of grooves on a workpiece made of *Ni-6Al-4V* alloy with coated and uncoated carbide tools at various cutting speeds: 50, 80 and 105 m/min, with feed rates of 0.1, 0.15 and 2 mm/tooth and cutting depths of 1, 1.5 and 2 mm accordingly. The effectiveness of the cutting tool was determined by the cutting tool life and quality of the machined surface. Based on the data obtained, it was concluded that the *PVD*-coated carbide tool has a higher tool life, amounting to a maximum of 11.5 minutes, and the surface roughness ***Ra*** is more sensitive to feed rate and cutting depth.

In [21], the authors showed that during high-speed machining, the optimal surface roughness value ***Ra*** = 0.51 μm is achieved with the following parameters: cutting speed $\boldsymbol{v}$ = 450 m/min, feed rate $\boldsymbol{f}$ = = 2100 mm/min, cutting depth $\boldsymbol{a_p}$ = 0.3 mm and machining step of 60%. The results of confirmatory tests with a value of less than 10% confirmed the results obtained. It is concluded that there is a good agreement with the experimental results. The results of this study show that the *Taguchi* method is able to analyze the complex features accompanying high-speed cutting processes.

In [22], *Ginting* & *Nouari* used carbide tools (*WC*+*Co* group) without coating under dry milling conditions with end mills at cutting speeds of 60, 75, 100, 115 and 150 m/min of *Ti-6242S* alloy, which is used for the aerospace industry. The axial and radial cutting depths were kept constant at 2.0 and 8.8 mm, and the feed rate values were 0.1 and 0.15 mm/tooth. Analysis of worn tools by scanning electron microscopy showed that the main causes of tool failure are wear on the flank surface and excessive chipping of the cutting edge.

In [10], *Huang*, *Li*, *Sun*, & *Ge* used a solid carbide end mill for conventional milling of *Ti-6Al-4V* alloy in dry cutting with different cutting speeds from 80 to 360 m/min, constant feed rate per tooth of 0.08 mm/tooth, axial cutting depth of 20 mm and radial cutting depth of 0.5 mm. The study of vibration during machining was carried out using an end mill with a variable tooth pitch using signal analysis methods and comparing the results with stable and unstable milling processes. It was found that vibration occurs due to the milling speed and impact forces, which leads to increased deformation hardening of the workpiece and thermal softening with increasing milling temperature. The optimal cutting speed was achieved at 160 m/min, which made it possible to achieve good surface quality and reduce milling forces at a given cutting speed.

Despite the relatively large number of publications on high-speed machining of titanium alloys, the work performed is of interest in view of the systematic approach to the description and disclosure of deformation phenomena through the study of elementary wear of the surfaces of cutting edges, the nature of the chip morphology and the quality of the surface layer after machining.

However, the comparatively small amount of data on the intensification of shaping by cutting products made of pure **α**-*Ti* for products with high strength with sufficient plasticity and viscosity, with high resistance to small plastic deformations, brittle and fatigue failure, used in the manufacture of cryogenic equipment and heat exchangers, makes this work relevant. In this regard, ***the purpose of this work*** is to study the effect of milling modes on the formation of wear on cutting edges and the features of chip formation during high-speed machining of **α**-*Ti Grade 2* alloy.

Based on a review of previously performed studies, the fundamental ***objectives*** of this study are the following points:

– to identify the nature and causes of the destruction of the cutting plates' coating during cutting, including the analysis of thermomechanical stresses in the working area, as well as to investigate the adhesion strength of coatings on the rake and flank surfaces in the cutting edge area;

– to study the effect of cutting speed on the formation of cutting edge defects, as well as to establish the role of built-up edges (sticks) in protecting or destroying the coating, depending on the adhesive properties of the system "machined material – coating – insert material";

– to determine the sources of heat generation and heat transfer mechanisms during cutting of *Ti Grade 2* alloy, as well as to find out the role of chips as a heat carrier in the formation of the temperature field on the rake surface;

– to investigate the morphology and mechanism of chip formation and analyze the effect of the temperature gradient along the chip thickness and the contact zone with the rake surface on its separation;

– to establish the influence of cutting modes (speed, feed rate, milling depth) on the geometric characteristics of the chip elements and on the conditions of chip destruction;

– to study the chip structure in the longitudinal section — the nature of the boundaries between the elements, their slope, the presence of braking zones at the rake surface, the distribution of plasticity over the chip thickness and the dependence of the boundaries on cutting modes;

– to evaluate the quantitative influence of machining parameters (speed, feed rate, milling depth) on chip parameters using correlation analysis, to identify the most significant factors.

Research methodology

Blank, experimental matrix and cutting tool

Ti Grade 2 samples measuring 80×40 mm were prepared from annealed sheet 10 mm thick (Fig. 1), produced according to *GOST 23755* (hardness 110–120 HB).

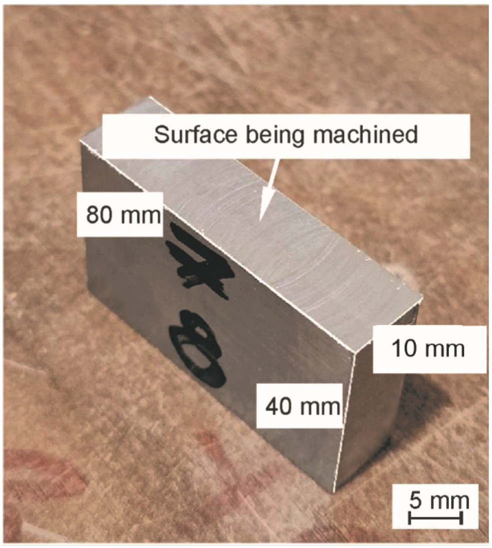

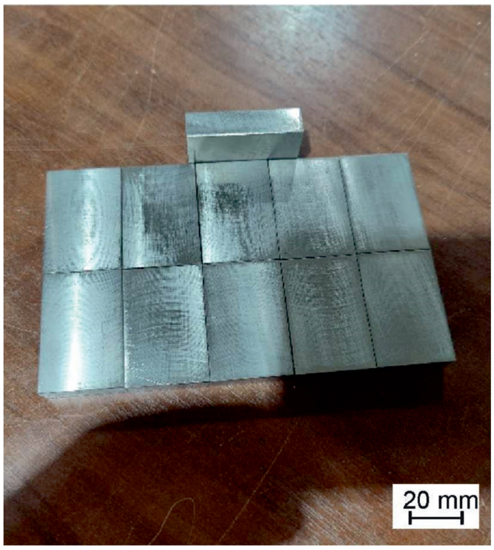

Fig. 1. Appearance of *Ti Grade 2* samples used for milling

A vise was used to clamp the samples, and the basing of the tool and the sameness (constancy) of the installation were ensured by basing on three planes. Each sample 10 × 40 mm with the machining area was marked and encrypted depending on the machining modes (Tables 1 and 2).

The machining was carried out on a machine *mod. 2440SF4* manufactured by the *Kuibyshev Machine Tool Manufacturing Association* (Russia). The machine belongs to a particularly high accuracy class – "C" according to *GOST 8-82*. This precision equipment is designed for the finishing of parts and has sufficient rigidity and precision of movement, which eliminates experimental errors caused by the dynamic characteristics of the equipment used. Symmetrical face milling was performed (see Fig. 2); the length of the cutting path in the feed direction during milling was at least 30 mm ($l_{milling} \geq 30$ mm), which made it possible to investigate elementary wear without labor-intensive resistance tests. The direction of rotation of the milling cutter and the movement during feeding were carried out according to the scheme of conventional milling, i.e. the direction of rotation (cutting speed $\boldsymbol{v}$) of the milling cutter coincided with the feed vector $\boldsymbol{f}$ at the beginning of cutting.

Table 1

Milling paramaters

Parameter	Level 1	Level 2	Level 3
Spindle speed $\boldsymbol{n}$, min^{-1}	800	1,590	2,390
Cutting speed $\boldsymbol{v}$, m/min	100	200	300
Feed rate $\boldsymbol{f}$, mm/min	50	100	–
Depth of cut $\boldsymbol{a}_p$, mm	0.2	0,4	–
Width of cut $\boldsymbol{a}_e$, mm	10		

Table 2

Correspondence of experiment numbers to variation levels

Experiment No.	Level ($\boldsymbol{v}$)	Level ($\boldsymbol{f}$)	Level ($\boldsymbol{a}_p$)
1	100	50 (0.02)	0.2
2			0.4
3		100 (0.04)	0.2
4			0.4
5	200	50 (0.01)	0.2
6			0.4
7		100 (0.02)	0.2
8			0.4
9	300	50 (0.007)	0.2
10			0.4
11		100 (0.014)	0.2
12			0.4

Note: to evaluate repeatability, experiments Nos. 1, 4, 5, 8, 9 and 12 were repeated twice.

In symmetrical milling, when the width of the sample is much smaller than the diameter of the milling cutter (see Fig. 2, *a*), the cutting plate of the milling cutter begins to cut with an impact and with a large uncut chip thickness. Therefore, the cutting edge perceives the greatest forces when it starts cutting. In this regard, it is rational to use a cutting edge with some rounding described by the radius $\boldsymbol{r}$, depending on the degree of wear of the cutting edges, and for a new tool – on the grain of the tool material, the rake and clearance angles, the presence of a wear-resistant coating on the cutting plate [23, 24].

In order to avoid the influence of rounding of the cutting edges on the cutting and wear parameters, all the plates used in the experiments were taken from the same batch, and then studied on *SEM*. Thus, all the cutting plates were identical and did not introduce third-party disturbing factors to the results obtained.

A *330-04000MKR03RD1206* body end mill (**ØD** = 40 mm, $\boldsymbol{l}$ = 70 mm, $\boldsymbol{L}$ = 179 mm, $\boldsymbol{z}$ = 3) with mechanical attachment of circular replaceable cutting plates (*INDEXABLE INSERT*) *RCKT 1204 MO-PM 4330* from *Sandvik Coromant* (Sweden) was used for milling (Fig. 3 and Table 3).

The support side of the inserts was marked in such a way that, after milling the sample, all three inserts could be rotated 90 degrees around the axis for subsequent use. Insert markings and milling modes (see Table 1) were grouped and encrypted in a single format, based on which an experiment matrix of the form *L12* (32+3) was compiled (Table 4).

Analytical equipment and research methods

Identification of the phases of the workpiece surfaces in the initial state was carried out on an X-ray diffractometer ***mod.*** *DRON-8H* manufactured by *NPP Burevestnik* (St. Petersburg) using *CuK*α radiation with a step of 0.05° and a holding time of at least 20 seconds per step [25, 26].

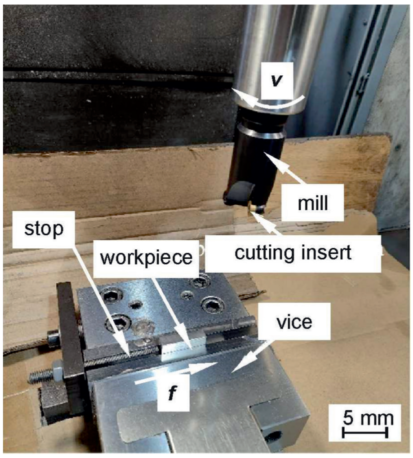

a

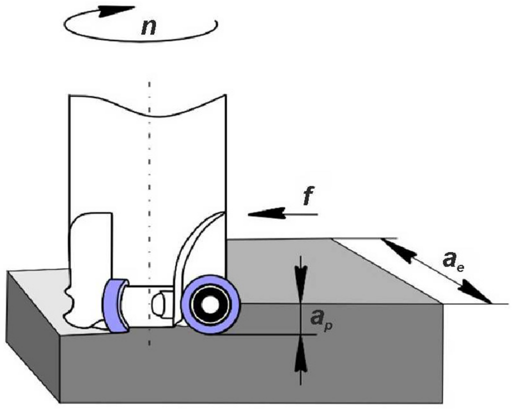

b

Fig. 2. Appearance of the milling zone (*a*) and milling scheme (*b*) showing the cutting elements

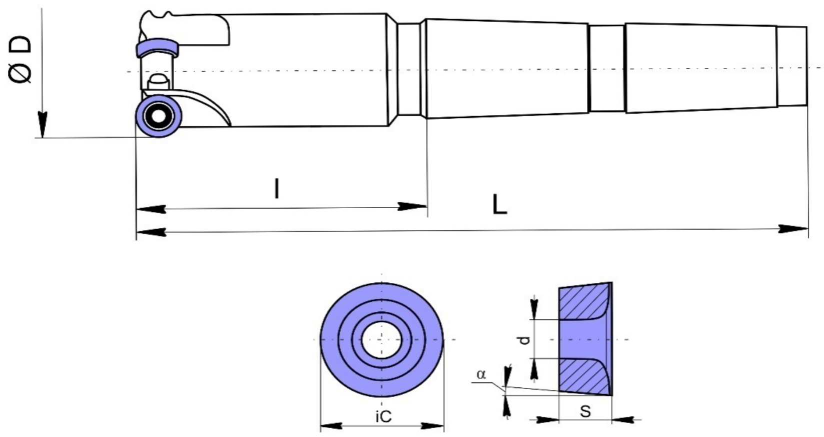

Fig. 3. Layout view and geometric parameters of the milling cutter and removable cutting insert

Table 3

Main characteristics of removable polyhedral inserts (*RPI*)

Alloy grade	Coating type	Inscribed circle diameter *iC*, mm	Insert thickness ***s***, mm	Clearance angle **α**, degree	Edge rounding radius **ρ**, mm
4330	Chemical vapor deposition (*CVD*)	12	4.762	15	0.03

Images of chips, as well as the working surfaces of replaceable cutting plates, and *CVD* coatings in their initial state and after wear were taken with high contrast and resolution (4,096 × 2,288 pixels per inch) on a *MIRA 3 LMU* scanning electron microscope from *Tescan* (Czech Republic), equipped with an energy dispersive microanalysis (*EDX*) attachment with a nitrogen-free detector *mod. Ultim MAX 40*. The measurement of microhardness by the *Vickers* method was carried out on a microhardness meter *mod. 502* from *Metolab* (Russia) at 0.098 N (10 grams) diamond indenter load with an exposure time of 10 seconds according to *ISO 6507-1:2005*.

For sample preparation, followed by *SEM* examination of the cross-section of coatings, grinding of cutting plates at an angle of 1–2° was used using Al_2O_3-based abrasive sheets with a grain size of *P2000* with the addition of a slightly alkaline aqueous solution.

Table 4

Experimental design matrix

Experiment No.	Level (*v*)	Level (*f*)	Level (a_p)
1	1	1	1
2	1	1	2
3	1	2	1
4	1	2	2
5	2	1	1
6	2	1	2
7	2	2	1
8	2	2	2
9	3	1	1
10	3	1	2
11	3	2	1
12	3	2	2

Data processing was performed using the principles of mathematical statistics. To analyze the relationship between a dependent variable and several independent variables, a multiple regression method was used, which was automated using the software *STATISTICA V. 8*. To understand possible relationships, correlation coefficients ***r*** were calculated (Table 5). It was assumed that if the calculated significance level of the model was $p < 0.05$, then the regression was assumed to be significant as a whole.

Table 5

Correlation coefficient ranges and their interpretation

Correlation coefficient range	Correlation
$0.01 < r \leq 0.29$	weak positive
$0.30 < r \leq 0.69$	moderate positive
$0.70 < r \leq 1.00$	strong positive
$-0.01 > r \geq -0.29$	weak negative
$-0.30 > r \geq -0.69$	moderate negative
$-0.70 > r \geq -1.00$	strong negative

Results and discussion

Initial condition of the cutting edges

X-ray diffraction has shown that the titanium alloy used in the study as the machined material consists of **α**-*Ti* without the presence of any other phases. The microhardness of the surface of the test sample was HV 0.1/10 248±15.

Fig. 4 shows the appearance of the initial condition of the working edges of the new cutting plate. There are chip-crushing curved grooves on the rake surface that prevent the formation of long solid chips and divide them into separate segments (elements) along their length during milling. For the ledges to work effectively, the chip thickness must be at least 1 mm.

The *CVD* coating is applied to the working surface of the cutting plates in two layers, as evidenced by *SEM* images in *BSE* mode (Fig. 5). The coating interface runs along the cutting edge, dividing it into two parts. A coating formed by two successive deposition procedures is present on the rake surface, whereas a coating formed by a single procedure is present on the flank surface. This is also evidenced by the elemental composition data obtained from the *EDX* attachment.

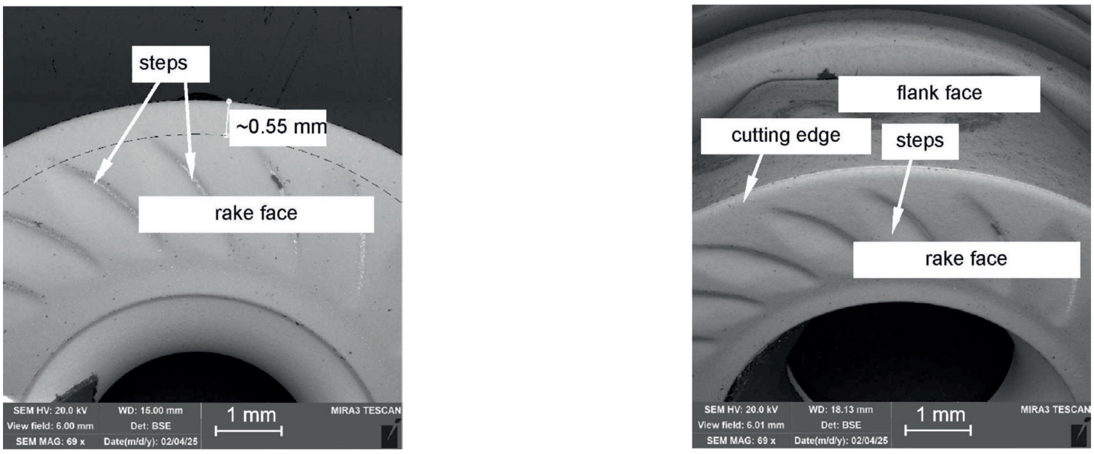

a *b*

Fig. 4. SEM-BSE images of a new *RCKT 1204 MO-PM 4330* cutting insert:

a – rake face view; *b* –) view along the bisector of the wedge angle

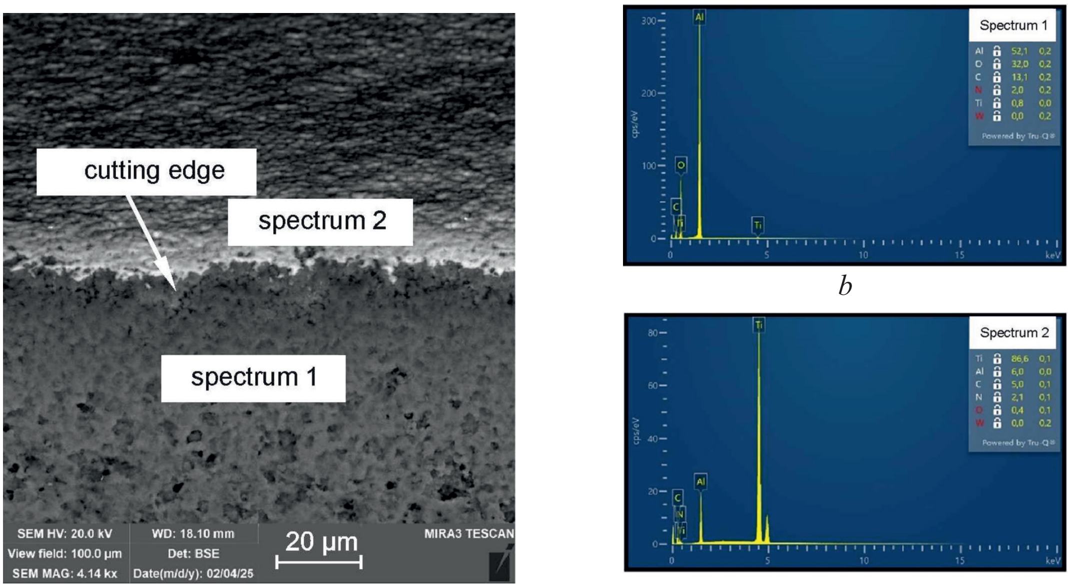

a *b* *c*

Fig. 5. SEM-BSE images of the coating near the cutting edge:

a – general view showing the locations of the spectra; *b* – spectrum No. 1; c – spectrum No. 2

The cross section and data on the chemical composition of the coating are shown in Fig. 6.

The coating is represented by a combination of layers consisting of an upper layer of Al_2O_3 with a thickness of ≈3.7 microns (normalized mass %, $Al = 44$; $O = 48$) and a combined transition layer of *TiCN*+*TiN* with a thickness of ≈4.4 µm (normalized mass %, $Ti = 57$; $N = 50$; $C = 9$). Thus, the total thickness of the *CVD* coating is ≈8.1 µm, which is typical for chemical deposition methods.

Wear of cutting edges

Using the cutting modes (see Table 1), a series of experiments on milling samples made of ***Ti Grade 2*** alloy was carried out.

The cutting plates selected during the experiment were examined on *SEM*. During their inspection, the wear of the coating, local chips and peeling, as well as the presence of adherents of the machined material on the cutting edges were analyzed (Fig. 7). Chipping refers to a section of the cutting edge or surface where, after contact with the material being machined, the continuity of the coating has been disrupted as a result of brittle fracture.

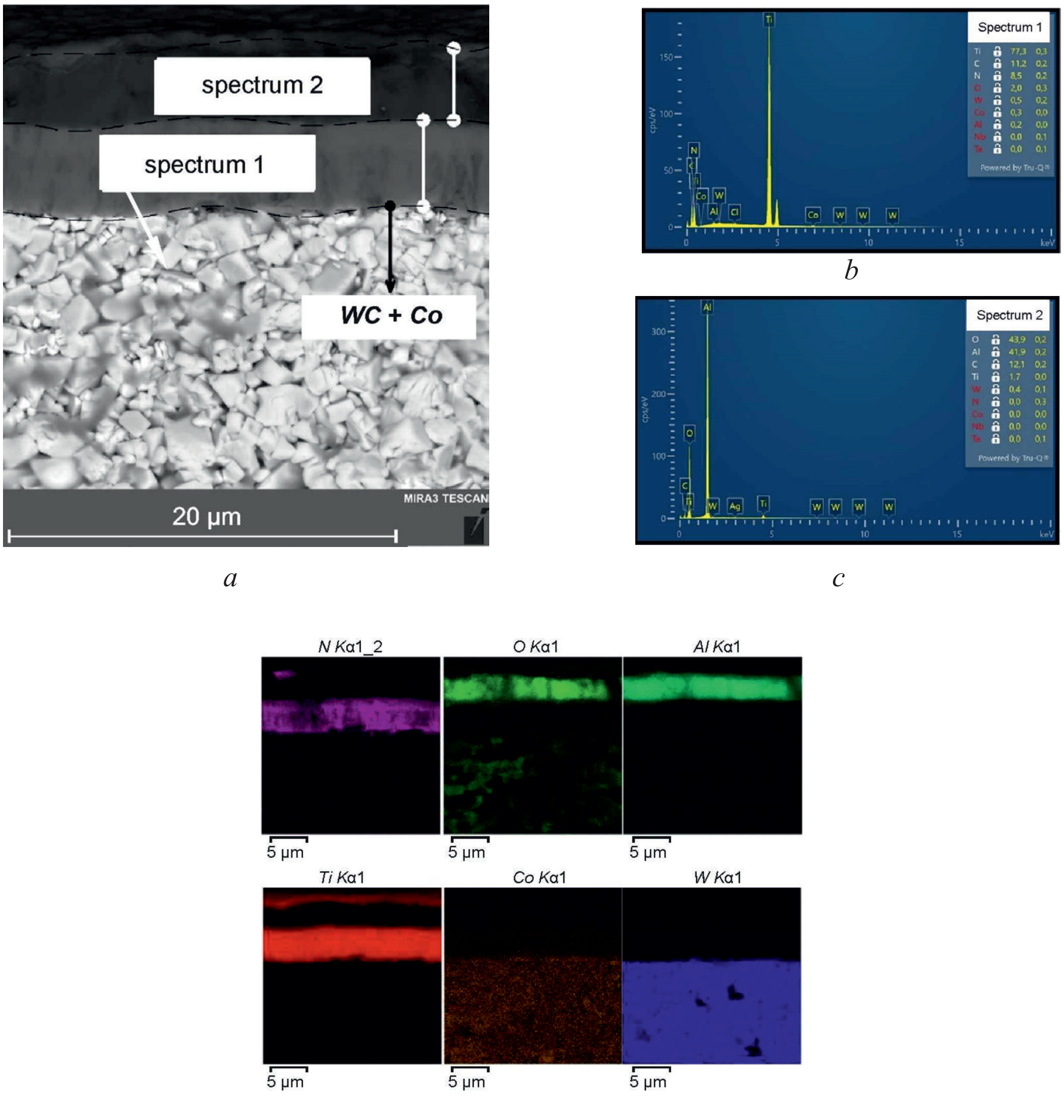

Fig. 6. SEM-BSE image of the coating in cross-section:
a – general view showing the locations of the spectra; *b*, *c* – spectra No. 1 and No. 2, respectively;
d – *XEDS* elemental maps

Fig. 7, *a* shows the condition of the rake and flank surfaces of the cutting plate, as well as the radius cutting edge, after a short milling without visible wear. The chamfer on the cutting edge, obtained during the manufacture of the indexable insert , is clearly visible in the photo. After longer milling with a milling depth of $\boldsymbol{a_p}$ = 0.4 mm, a wear zone appears on the chamfer of the flank surface, but it also captures a small area of the rake surface adjacent to the cutting edge.

At a cutting speed of 100 m/min and a constant feed rate of 50 mm/min, an increase in the cutting depth $\boldsymbol{a_p}$ from 0.2 mm to 0.4 mm in experiment No. 2 leads to an expansion of the chip contact boundaries with the cutting edge, which is confirmed by a characteristic image (see Fig. 7, *b*). The width of the chip contact zone with the rake surface is ≈1.8 mm along the length of the curved part of the cutting edge.

Fig. 7, *d* shows that with a slightly shorter milling time, wear develops more intensively in the area related to the auxiliary cutting edge of the indexable insert, i.e. in contact with the cutting surface bordering the already machined surface of the sample. When the cutting speed is increased to 200 m/min, local chips appear on the rake surface (see Fig. 7, *e*) and the cutting edge (see Fig. 7, *f*, *g*), which are more visible when the milling depth is increased to $\boldsymbol{a_p}$=0.4 mm (see Fig.7, *f*) and the feed $\boldsymbol{f}$ = 100 mm/min (see Fig. 7, *g*). In our opinion, this is due to the temperature increasing with the cutting speed and the increased adhesion of the machined material to the material of the cutting plates.

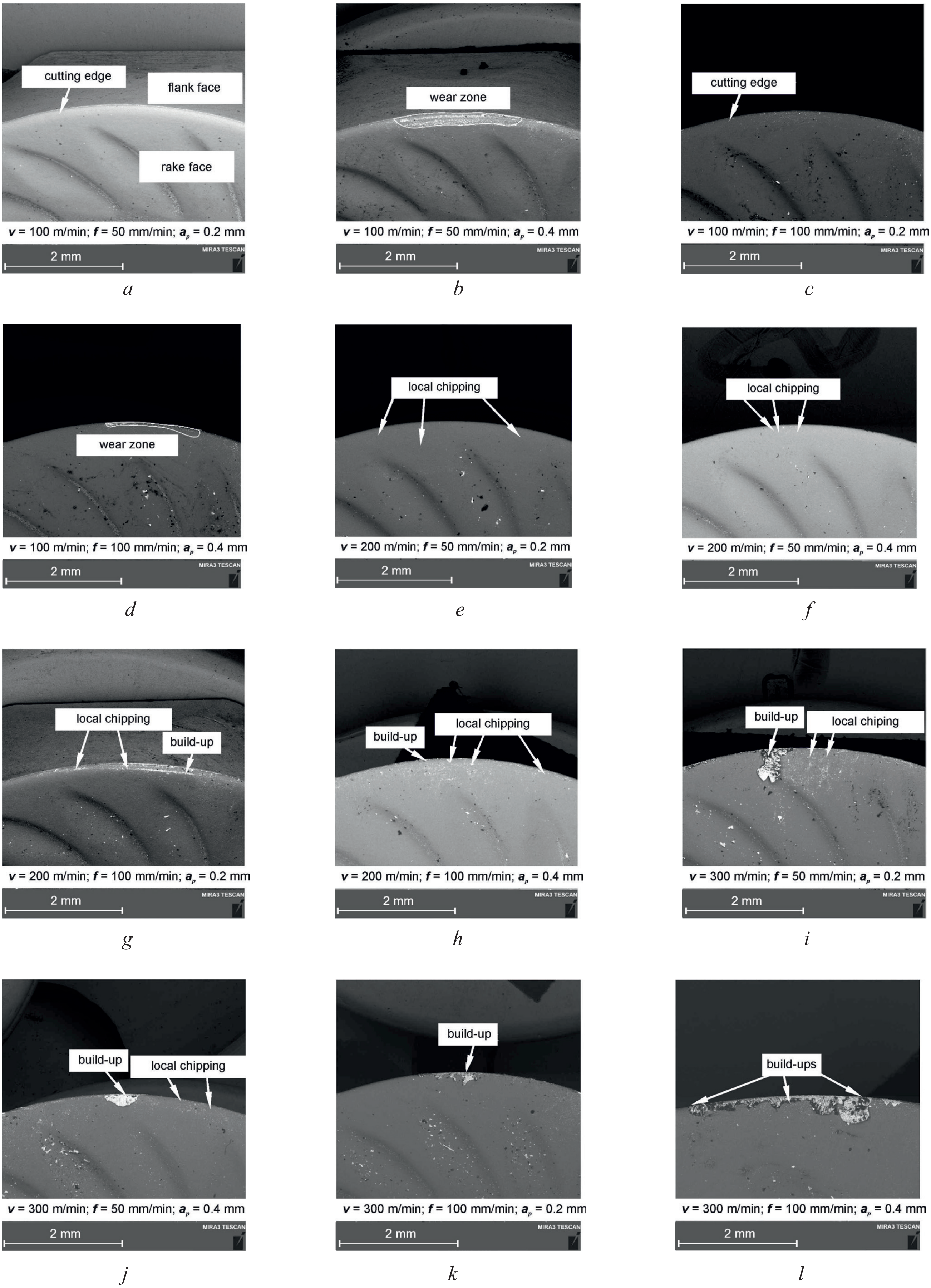

Fig. 7. SEM images of the cutting edges of inserts after milling of *Ti Grade 2* under different conditions

This assumption is supported by an increase in the intensity of chips adhesion (sticking of the machined material) with an increase in cutting speed to 300 m/min (see Fig. 7, *i*, *j*, *k*).

With a cutting depth of a_p = 0.4 mm, dotted areas with chips adhesion begin to form on the rake surface (Fig. 8). In turn, on the flank surface, the material sticking are represented by a continuous layer no more than 0.1 mm wide.

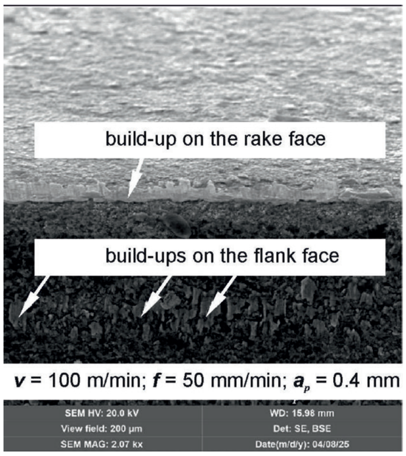

Fig. 8. SEM image fragment of the cutting edge of an insert with built-up material on the flank and rake surfaces

A similar wear pattern is observed at the same speed and with an increase in feed rate from 50 mm/min to 100 mm/min (experiment No. 4, see Fig. 7, *d*), however, in this case, the wear zone is clearly manifested with an offset relative to the geometric center of the cutting plate. This phenomenon is observed with the conventional scheme of milling, when the chips begin to deform intensively with a change in the uncut chip thickness from zero to the maximum a_p value, which subsequently leads to its twisting.

As the cutting speed increases from 100 m/min to 200 m/min (experiments Nos. 5 and 6, see Fig. 7, *e*, *f*), local chips form on the rake surface of the cutting plates, which, all other things being equal, indicates an increase in temperature in the contact zone of the cutting edges of the plates with the material being machined. Thus, thermomechanical stresses of a magnitude exceeding compressive strength are formed in the working area of the coating (Fig. 9).

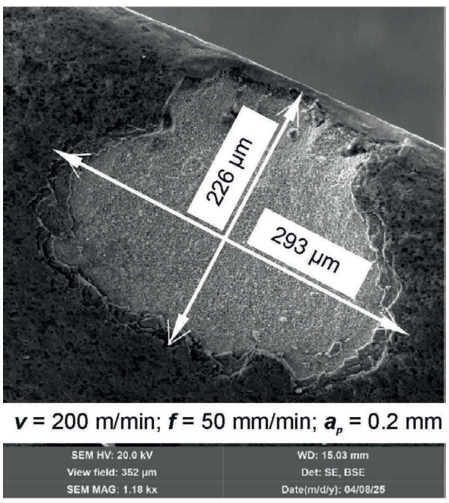

Fig. 9. SEM image fragment of the rake face of a cutting insert with coating fracture and delamination

At the same time, the coating on the flank surface remains intact and has the appearance of a thin wall, which indicates insufficient strength of the coatings on the rake and flank surfaces, i.e. on the cutting edge.

An increase in feed from 50 mm/min to 100 mm/min at a cutting speed of 200 m/min leads to an intensification of the total chipping area, as well as sticking of the machined material (experiment No. 7, see Fig. 7,*g* and Fig. 10).

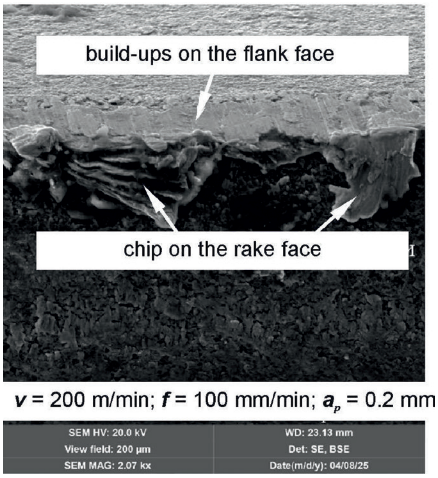

Fig. 10. SEM image fragment of the cutting edge of an insert with built-up material on the flank face and chip on the rake face

A further increase in the cutting speed from 200 m/min to 300 m/min (experiments No. 9-12, see Fig. 7, *h–j*). demonstrates the appearance of local chips on the cutting edge, reaching a length of ≈ ≈ 0.3–0.4 mm. Also, the sticking of the machined material on the rake surface are significantly increased in comparison with previous milling modes. Upon closer examination of the cutting edge, it can be seen that it is hidden under layers of adhering (sticking) chips, which is typical for the processes of appearance of a build-up edge (outgrowth). The outgrowth overhanging the flank surface, being hardened by the machined material during thermomechanical influence, on the one hand, protects the cutting edge from direct contact with the machined material, and on the other hand, when it is torn off, increased wear of the surface layers of the coating occurs as a result of adhesion (Fig. 11). Also, the presence of an outgrowth negatively affects the roughness of the machined surface.

The significantly protruding sticking above the rake surface (see Fig. 11, *a*) is caused by the processes occurring at the moment of feed interruption and chip formation at the end of cutting, when the cutting edge scrapes along the transient surface without chip formation, which was supposed to remove this protruding volume in the form of chips.

An increase in the width of the material sticking on the rake surface compared to its width at the cutting edge (see Fig. 11, *b*) indicates the broadening of the sticking when moving away from the cutting edge, which indirectly indicates significant resistance to chip movement. Usually, the length of the sticking section on the rake surface corresponds to the length of the chip's plastic contact with the rake surface [27, 28].

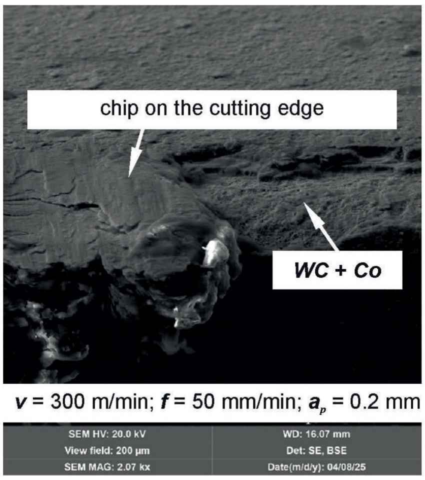

a

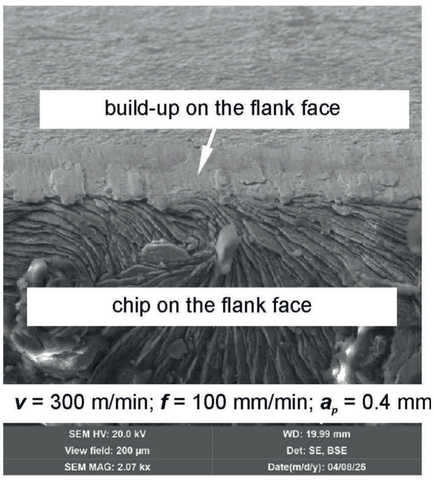

b

Fig. 11. SEM image fragments of the cutting edges of inserts with built-up edges and demonstration of wear-resistant coating fracture:

a – Experiment No. 9; *b* – Experiment No. 12

Table 6 summarizes the description of individual representative images that show, at an enlarged scale, coating wear, chipping and localized adhesion.

Table 6

Condition of cutting edge plates after milling

Experiment No.	Level (***v***)	Level (***f***)	Level (a_p)	Condition of edges
1	100	50	0.2	no wear
2			0.4	wear zone and built-up material
3		100	0.2	local chipping
4			0.4	wear zone and built-up material
5	200	50	0.2	local chipping
6			0.4	local chipping
7		100	0.2	local chipping and built-up material
8			0.4	local chipping and built-up material
9	300	50	0.2	local chipping and increased built-up material
10			0.4	local chipping and increased built-up material
11		100	0.2	local chipping and built-up material
12			0.4	local chipping and increased built-up material

Abrasion of the coating (abrasive wear) was not observed throughout the experiments.

The heat source during cutting is the heat of deformation, and the chips act as a heat carrier, which transfers heat to the rake surfaces only from the layers lying in close proximity to the contact zone. It is worth noting that with this phenomenon, a significant part of the heat received by the cutting wedge is discharged into its body and into the environment. According to [29], the temperature in the cutting zone can reach 500 to 650 ºC in the cutting speed range of 100–700 m/min for easy-to-machine groups of titanium alloys and significantly depends on the wear of the cutting edges, especially along the flank surface, when it can reach 1,200 ºC for difficult-to- machine groups of titanium alloys [2].

Since the deformation processes during cutting are directly related to the amount of heat generated during milling, the plastic flow of the chip being cut increases with increasing cutting speed and increases the total adhesion area. The largest amount of chips remaining on the rake surface of the cutting plates is observed at ***v*** = 300 m/min; ***f*** = 100 mm/min and a_p = 0.4 mm, which are the limits in this study.

Chip morphology

A detailed consideration of chips as wear products in the process of elastic-plastic deformation during cutting contributes to the understanding of the physical phenomena accompanying the wear of cutting edges. As part of this work, sample preparation of the chips was carried out, followed by *SEM* at the same magnifications (Fig. 12).

In the top view, the chips have the shape of disk sectors, on the inner surfaces of which there are notches (teeth) indicating the formation of chip elements that are tightly welded to each other. This arrangement of the teeth indicates a more plastic state of the chips on the outside, formed at the tip of the cutting edge, where the temperature is higher. The inner side cools faster because it is in contact with the colder part of the rake surface of the circular cutting plate. The rupture of the continuous chips into sectors can begin both from the inside (see Fig. 12, *b*) and from the outside (see Fig. 12, *f*, *g*, *k*, *l*), and on both sides simultaneously (see Fig. 12, *e*, *i*, *j*).

The distance between the vertices (teeth) of the elements is approximately the same for the same sector, but may vary for different sectors even with the same cutting modes (see Fig. 12, *a*, *b*). At a cutting speed of 100 m/min, the appearance is approximately the same with different feed and cutting depth, but with an

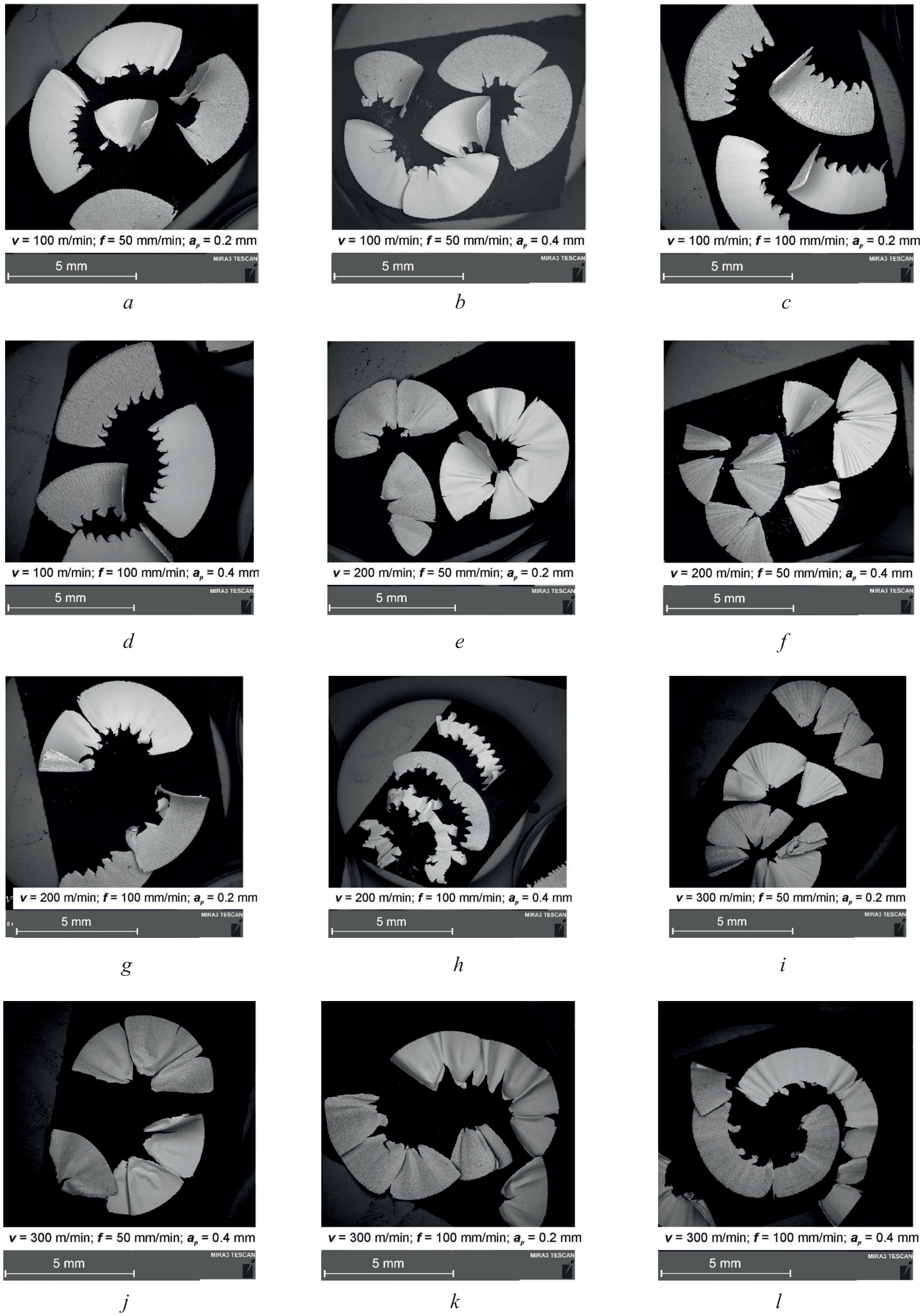

Fig. 12. SEM images of chips obtained under different conditions

increase in feed rate f_{min} to 100 mm/min, the height of the teeth increases and they become more pronounced (see Fig. 12, *a*, *c*). Increasing the milling depth a_p from 0.2 to 0.4 mm has no visible effect on the pitch of the teeth and their height (see Fig. 12, *c*, *d*).

An increase in the cutting speed to 200 m/min with a feed rate of 50 mm/min leads to the disappearance of the teeth (see Fig. 12, *e*, *f*), but with a feed rate of 100 mm/min and a milling depth of 0.2 mm they become noticeable again (see Fig. 12, *g*), and with a milling depth of 0.4 mm the pitch between the teeth increases (see Fig. 12, *h*), the sectors become less curved, sometimes even shapeless (see Fig. 12, *h* bottom left), and some have teeth on both sides (see Fig. 12, *h* top). This indicates the uncertainty of plastic deformation, apparently caused by a change in the temperature gradient specific to high-speed milling.

Increasing the cutting speed to 300 m/min at a feed rate of 50 mm/min again leads to the disappearance of the teeth (see Fig.12, *i*, *j*), the sectors become larger and less curved. Increasing the feed to 100 mm/min at a milling depth of 0.2 mm leads to sector splicing and the teeth that appear in this form have a greater height (see Fig. 12, *k*). Increasing the milling depth to 0.4 mm leads to even greater sector splicing and the teeth disappear, but sometimes occasionally appear as thin protrusions of great height (see Fig. 12, *l*).

It can be generally concluded that as the cutting speed increases, the cutting temperature increases, which leads to an increase in chip ductility. An increase in feed rate leads to an increase in the volume of the plastically deformable machined material, which causes a break between elements of the continuous chip on the inside due to exceeding the tensile strength of the machined material.

The length of the chip's contact with the rake surface when machining titanium alloys forming serrated or even discontinuous chips is much shorter than when machining steel. This also explains the formation of large shear angles with low chip shrinkage (chip ratio) during cutting of titanium alloys, as a rule, its chip ratio along the length is close to unity. This can be seen from the values of the chip ratio of various grades of titanium and hard alloys, as well as the dependence of the longitudinal deformation of the chips on the cutting speed and feed rate.

In some cases, as a result of the absorption of oxygen and nitrogen from the air during the machining of titanium alloys, the so-called negative chip shrinkage (chip ratio) is obtained, i.e. the length of the chips formed is longer than the length of the cutting path. The decrease in chip shrinkage with increasing cutting speed is also explained by a sharp decrease in the friction forces of the chips with the rake surface. Titanium alloys are characterized by high coefficients of friction at temperatures below 200 ºC, which limits their use for movable joints. However, when cutting, the temperature of the contact chip layer increases to 600–1,200 ºC due to the low thermal conductivity of titanium alloys and the heat concentration in a small volume of the primary plastic deformation zone. This leads to a pseudo-liquid state of the contacting chip layer and a very low coefficient of friction on the rake surface and on the wear chamfer on the flank surface. The low coefficient of friction is also indicated by the very small angle of inclination of the boundaries of the chip elements, which are located almost perpendicular to the cutting surface of the chip (the rake surface of the tool) (Fig. 13), i.e. there is no braking on the rake surface of the tool.

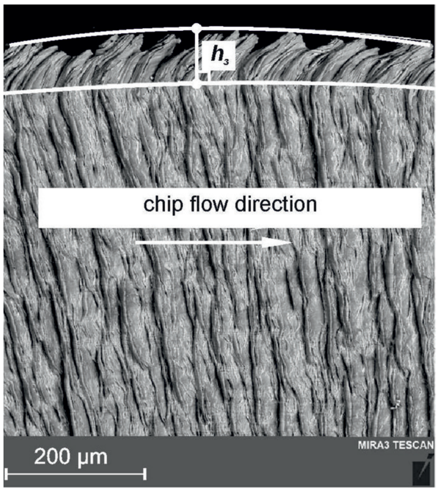

Fig. 13. Measurement scheme for parameter h_3 using *SEM* (Experiment No. 1)

As the uncut chip thickness increases, the average conditional coefficient of friction $\mu_{average}$ decreases [2]. This is due to an increase in heat generation as the uncut chip thickness increases. As the temperature increases, the coefficient of thermal conductivity of titanium alloys increases significantly, but this still does little to compensate for the heat concentration in the zone of primary plastic deformation and on the contact surfaces of the tool.

The short length of the chip's contact with the rake surface during machining of titanium alloys leads to the fact that the entire load is distributed over a very small area of the rake surface, which leads to a decrease in the cutting tool life and rapid destruction of its cutting edge. This is also facilitated by the formation of solid titanium carbide during cutting, if the carbon content in the titanium alloy is more than 0.2 %, since carbon is dissolved in the titanium alloy only up to 0.2 %.

With an increase in the cutting speed due to the occurrence of a very high temperature in the deformed zone, the process of absorption of gases (oxygen and nitrogen) from the air by this layer is significantly intensified, which leads to an increase in the role of embrittlement and the development of shear deformation [30, 31].

Thus, the chips obtained under high-speed dry milling conditions can be classified in detail according to the description in Table 7.

Table 7

Description of features of *Ti Grade 2* chips

Experiment No.	Features of chips
1	typical (continuous chip): chip elements are clearly distinguishable but tightly pressed and welded to each other; the elements are thin; the protrusions (ridges) on the outer side of the chip are of small height
2	
3	
4	
5	crack development on both sides
6	increase in length and intensity of crack development
7	
8	tendency of the narrow part to curl
9	crack development on both sides; waviness on the chip surface
10	increase in length and appearance of waviness on the chip surface
11	
12	formation of individual irregular outgrowths

* Thickness reduction: an increase in deformation density is observed under modes 4, 8, and 12.

Experiment No. 1. The chip elements are clearly distinguishable, but they are tightly pressed and welded to each other. The elements are of small thickness; the protrusions (scallops) on the outside of the chips are of small height and the boundaries between the elements are straight and, near the cutting edge, almost perpendicular to the rake surface, slightly inclined.

Experiment No. 2. The chip elements are indistinctly distinguished, especially in the middle and, near the cutting edge, visually more tightly pressed and welded to each other. The elements are small in thickness, the boundaries between the elements are straight and almost perpendicular to the rake surface, and the protrusions (scallops) on the outside of the chips are small in height and almost the same as in No. 1.

Experiment No. 3. The chip elements practically do not differ in the middle and, near the cutting edge,, forming one whole; on the outside the elements are thicker than those in Nos. 1 and 2, the boundaries between the elements are blurred and strongly curved. Near the cutting edge, they are perpendicular to the rake surface, slightly curved away from the cutting edge, and significantly curved to the opposite side on the outside.

Experiment No. 4. The chip elements are practically indistinguishable in the middle and, near the cutting edge, of the chip, forming one whole; the boundaries between the elements are blurred and strongly curved. Near the cutting edge, they are perpendicular to the rake surface, slightly curved above. On the outside, the elements are smaller in thickness compared to those in No. 3, the protrusions (scallops) on the outside of the chips are higher than in the other chips, and the chip elements are clearly distinguished.

Experiment No. 5. The chip elements are clearly distinguishable, but they are very tightly pressed and welded to each other. The elements are small in thickness, the boundaries between the elements are straight and, near the cutting edge, almost perpendicular to the rake surface, slightly inclined, and the protrusions (scallops) on the outside of the chips are small and smaller than those in No. 1. In this mode, for the first time in the experiments, the development of cracks in the chips from two sides is observed.

Experiment No. 6. The chip elements are not very clearly distinguishable, they are very tightly pressed and welded to each other. The elements are small in thickness, the boundaries between the elements are straight and, near the cutting edge, almost perpendicular to the rake surface, slightly inclined, the protrusions (scallops) on the outside of the chips are not prominent and are smaller than those of No. 5. There is a small crack along the outer side – in other words, the crack starts on the outer side.

Experiment No. 7. The chip elements are indistinctly distinguished, especially in the middle and near the cutting edge, and are more tightly pressed and welded to each other. The elements are small in thickness, the boundaries between the elements are straight and, near the cutting edge, almost perpendicular to the rake surface, slightly inclined. The chip elements are different, almost the same as those of No. 2, but smaller in height.

Experiment No. 8. The chip elements are different in the middle and, near the cutting edge,, they are more tightly pressed and welded to each other. The elements are small in thickness, the boundaries between the elements are straight and, near the cutting edge, almost perpendicular to the rake surface, slightly inclined away from the cutting edge. The protrusions (scallops) on the outside of the chip are quite high compared to those in the other chips and are almost the same as in No. 1. There are no cracks, but there is a tendency for the narrow part to twist.

Experiment No. 9. The chip elements are not very clearly distinguishable, they are very tightly pressed and welded to each other. The elements are small in thickness, the boundaries between the elements are straight and, near the cutting edge, almost perpendicular to the rake surface, slightly tilted, after the fracture they are tilted in the opposite direction. There are practically no protrusions (scallops) on the outside of the chips. There is a separation of the chips along their length (a fracture on the outside) and waviness on the outer surface of the chips.

Experiment No. 10. The chip elements are indistinctly distinguished, especially in the middle and at the cutting part, they are more tightly pressed and welded to each other. The elements are small in thickness, the boundaries between the elements are straight and, near the cutting edge, almost perpendicular to the rake surface, slightly inclined. There are no protrusions (scallops) on the outside of the chips; cracks develop from the outside and there is waviness on the outer surface of the chips.

Experiment No. 11. The chip elements are indistinctly distinguished, especially in the middle and at the cutting part, they are more tightly pressed and welded to each other. The elements are small in thickness, the boundaries between the elements are straight and, near the cutting edge, almost perpendicular to the rake surface, the protrusions (scallops) on the outside of the chip are of very small height compared to those in the other chips, almost the same as in No. 7, but smaller in height.

Experiment No. 12. The chip elements are clearly distinguishable, but they are very tightly pressed and welded to each other. The elements are small in thickness, the boundaries between the elements are straight and, near the cutting edge, almost perpendicular to the rake surface, slightly inclined away from the cutting edge. The protrusions (scallops) on the outside of the chips are quite high, but smaller than those of No. 1, 5. The formation of separate irregular processes (protrusions) is observed, as in experiment No. 8.

In general, it is worth noting that modes 4, 8, and 12 (the limit modes for their group) show an increase in strain density.

The chip continuity coefficient [32–36] was estimated by estimating the ratio of the normal chip width h_2, measured from the outer surface to the place where cracks appear on the inner surface, to the total chip width h_1 (Fig. 14). The chip continuity coefficient reflects the transition from continuous chips to discontinuous. The higher the chip continuity coefficient, the closer it is to the continuous (solid) chips.

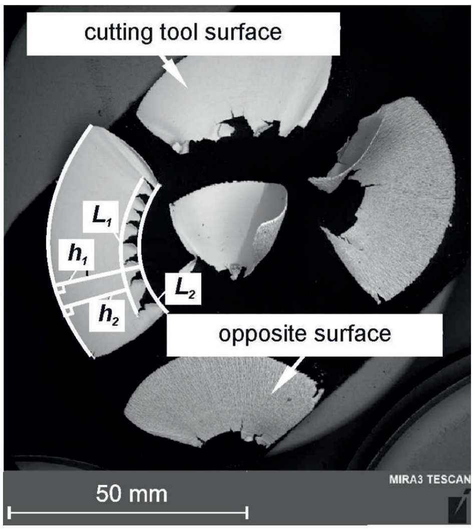

Fig. 14. Measurement scheme for parameters h_1, h_2, L_1 and L_2, for calculating the chip continuity coefficient

By measuring the parameters h_1, h_2, L_1 and L_2, Table 8 was generated, on the basis of which statistical processing was performed and correlation coefficients between chip parameters and machining modes were calculated.

Table 8

Geometric dimensions of characteristic chip elements

Experiment No.	h_1, mm	h_2, mm	Chip continuity coefficient h_2/h_1	L_1, mm	L_2, mm
1	1.82±0.09	1.37±0.16	0.75	0.48	0.56
2	2.14±0.11	1.73±0.21	0.81	0.35	0.50
3	2.10±0.12	1.53±0.2	0.73	0.52	0.37
4	2.20±0.11	1.74±0.21	0.79	0.51	0.39
5	2.04±0.15	1.54±0.15	0.76	0.67	0.45
6	2.15±0.16	1.60±0.22	0.74	0.41	0.25
7	2.07±0.09	1.64±0.16	0.79	0.42	0.39
8	0.95±0.1	0.69±0.08	0.73	0.35	0.29
9	1.90±0.1	1.15±0.16	0.60	0.74	0.30
10	2.16±0.08	1.82±0.16	0.84	1.11	0.47
11	2.00±0.09	1.21±0.22	0.61	0.49	0.66
12	1.63±0.12	1.32±0.14	0.81	0.56	0.50

The milling depth a_p ($r = 0.55$) has the greatest effect on the chip continuity coefficient, while a moderate positive correlation is observed. In turn, the cutting speed has a weak negative effect ($r = -0.31$), and the feed rate effect in the range from 50 to 100 mm/min is negligible ($r = -0.04$) and can be ignored.

The L_1 parameter, which characterizes the crack opening step from the inner surface of the chip, depends more on the milling speed ($r = 0.52$) than on the feed ($r = -0.37$), and the cutting depth has no effect at all ($r = -0.01$).

In the range of all high-speed milling modes (see Table 1 and 2), no stable relationship has been established between the milling parameters and the L_2 parameter, which characterizes the pitch of the protrusions on the inner surface of the chip after the formation of cracks along the length.

When studying the deformation bands of the chips, the height of the h_3 protrusions was measured according to the scheme (see Fig. 13).

The dimensions of the height parameters of the h_3 protrusions are shown in Table 9.

Table 9

Geometric dimensions of chip protrusions

Experiment No.	Thickness of protrusions on the upper part of the chip h_3, μm
1	72.05±12.6
2	63.18±11.1
3	114.47±22.3
4	113.29±16.9
5	36.32±5.6
6	28.37±4.1
7	55.40±8.9
8	61.73±6.1
9	15.05±3.4
10	27.09±4.1
11	40.44±9.3
12	38.81±9.2

When evaluating the correlations between the cutting modes and the height parameters of the $\boldsymbol{h}_3$ protrusions, it was found that the cutting speed ($\boldsymbol{r}$ = −0.81) has the greatest effect on the deformation of the protrusions, which has a stable strong negative correlation. This indicates that when the cutting speed increases in the range from 100 to 300 m/min, the height of the $\boldsymbol{h}_3$ protrusions decreases. A moderate correlation is observed in determining the effect of feed ($\boldsymbol{r}$ = 0.49). In turn, the cutting depth, other things being equal, has absolutely no effect on milling modes, and the correlation coefficient tends to zero.

Conclusions

1. Thermomechanical stresses are formed in the working area of the coating, the magnitude of which exceeds the compressive strength of the coating or its adhesion to the surface of the cutting plate, which leads to significant coating defects. The coating on the flank surface remains intact after the coating on the rake surface is destroyed and has a thin wall, which indicates insufficient bonding strength of the coatings on the rake and flank surfaces, i.e. on the cutting edge, and the integrity of this wear-resistant coating of the flank surface in the form of a thin wall indicates that there are no normal contact stresses on the flank surface near the cutting edge, and a stagnant zone occurs on the cutting edge.

2. Increasing the cutting speed from 200 m/min to 300 m/min leads to the appearance of local scuffing and scratches on the cutting edge, reaching a length of 0.3–0.4 mm. The sticking of the machined material on the rake surface are also significantly increased. The cutting edge is hidden under layers of sticky chips, which is typical for rough cutting processes. The sticking of the machined material on the flank surface, hardened by thermomechanical action as an outgrowth (built-up edge), on the one hand, protects the cutting edge from direct contact with the machined material, and on the other hand, when it is removed, increased peeling of the coating occurs as a result of good adhesion of the machined material to the coating and poor adhesion of the coating to the base material of the cutting plate.

3. The heat source during cutting is the heat of deformation in the primary zone of plastic deformation, and the chips act as a heat carrier, which can transfer heat to the rake surface only from the layers lying in the immediate vicinity of the contact zone. The heat generation from the friction of the chips with the rake surface is very small, because the coefficient of friction on the rake surface when cutting titanium alloy *Ti Grade 2* is small, which is indirectly indicated by the perpendicularity of the boundaries of the chip elements relative to the rake surface.

4. In top view of the chip, it have the shape of disk sectors, on the inner surfaces of which there are notches (teeth) indicating the formation of chip elements that are tightly welded to each other. This arrangement of the teeth indicates a more plastic state of the chips on the outside, formed at the top of the cutting edge, where the temperature is higher. The inner side cools faster because it comes into contact with the colder part of the rake surface of the circular cutting plate. The separation (destruction) of chips with the appearance of sectors can begin from the inside or from the outside, as well as from both sides simultaneously.

5. The teeth on the inside of the chips in the top view can change their size and shape depending on the cutting mode. Increasing the cutting speed to 300 m/min with a feed rate of 50 mm/min leads to the disappearance of the teeth, the sectors become larger and less curved. Increasing the feed to 100 mm/min at a milling depth of 0.2 mm leads to sector splicing, resulting in higher tooth heights. Increasing the milling depth to 0.4 mm leads to even greater splicing of the sectors, the teeth disappear, but sometimes appear as thin protrusions of very high height.

6. In the longitudinal section, the chip elements are tightly pressed and welded to each other, of small thickness, in most cases the boundaries between the elements are straight, at the rake surface they are slightly inclined from the cutting edge, i.e. there is braking when it moves along the rake surface. In most cases, the borders are clearly distinguishable, but in some cases, depending on the cutting mode, they are blurred in the middle and curved ($\boldsymbol{v}$ = 100 m/min, $\boldsymbol{f}$ = 100 mm/min, $\boldsymbol{a}_p$ = 0.2 mm): at the rake surface, the borders are slightly curved away from the cutting edge (that is, there is braking on the rake surface), slightly higher this slope is significantly greater (the higher lying layers of chips move faster than the lower ones,

i.e. there is an intermediate layer of metal with greater ductility than the lower one), and above they are significantly curved in the opposite direction, i.e. towards the cutting edge, which is due to the formation of chip elements in the area the conditional shear plane. The borders of the elements can stand out clearly, but sometimes indistinctly, depending on the cutting mode, especially in the middle and near the rake surface.

7. The milling depth (r = 0.55) with a moderate positive correlation has the greatest effect on the chip continuity coefficient. In turn, the cutting speed has a slight negative effect (r = −0.31), and the impact of feed rate in the range from 50 to 100 mm/min is insignificant (r = −0.04) and can be ignored. The L_1 parameter, which characterizes the degree of crack opening from inside the chip, depends more on the milling speed (r = 0.52) than on the feed rate (r = −0.37), and the cutting depth does not affect it at all (**r** = −0.01). When evaluating the correlations between the cutting modes and the height parameters of the h_3 protrusions, it was found that the cutting speed (r = −0.81) has the greatest effect on the deformation of the protrusions, which has a stable strong negative correlation. This indicates that as the cutting speed increases in the range from 100 to 300 m/min, the height of the h_3 protrusions decreases. When determining the effect of feed rate, a moderate correlation is observed (r = 0.49). In turn, the cutting depth has absolutely no effect when other milling conditions are equal, and the correlation coefficient tends to zero.

References

1. Komanduri R. Some clarifications of the mechanics of chip formation when machining titanium alloys. *Wear*, 1982, vol. 76, pp. 15–34. DOI: 10.1016/0043-1648(82)90113-2.

2. Kozlov V.N., Zhang J.Y., Letshiner E., Zhao W.Z. Influence of cutting tool wear on contact stresses and temperature distribution in titanium alloy machining. *Key Engineering Materials*, 2017, vol. 743, pp. 252–257. DOI: 10.4028/www.scientific.net/KEM.743.252.

3. Kozlov V.N., Zhang J.Y. Strength of cutting tool in titanium alloy machining. *Key Engineering Materials*, 2016, vol. 685, pp. 427–431. DOI: 10.4028/www.scientific.net/KEM.685.427.

4. Liu H., Sun Y., Geng Y., Shan D. Experimental research of milling force and surface quality for TC4 titanium alloy of micro-milling. *International Journal of Advanced Manufacturing Technology*, 2015, vol. 79, pp. 705–716. DOI: 10.1007/s00170-015-6844-5.

5. Oliaei S.N., Karpat Y. Investigating the influence of built-up edge on forces and surface roughness in micro scale orthogonal machining of titanium alloy Ti6Al4V. *Journal of Materials Processing Technology*, 2016, vol. 235, pp. 28–40. DOI: 10.1016/j.jmatprotec.2016.04.010.

6. Feng J., Sun Z., Jiang Z., Yang L. Identification of chatter in milling of Ti-6Al-4V titanium alloy thin-walled workpieces based on cutting force signals and surface topography. *International Journal of Advanced Manufacturing Technology*, 2016, vol. 82, pp. 1909–1920. DOI: 10.1007/s00170-015-7509-0.

7. Bogoljubova M., Afonasov A., Kozlov V., Sumtsova O. Mathematical simulation and optimization of cutting modes in turning of titanium alloy workpieces. *IOP Conference Series: Materials Science and Engineering*, 2016, vol. 124, p. 012045. DOI: 10.1088/1757-899X/124/1/012045.

8. Rahman M., Wang Z.G., Wong Y.S. A review on high-speed machining of titanium alloys. *JSME International Journal. Series C*, 2006, vol. 49, pp. 11–20. DOI: 10.1299/jsmec.49.11.

9. Li L., He N., Xu J.H. Experimental study on high speed milling of Ti alloys. *Materials Science Forum*, 2004, vol. 471–472, pp. 414–418. DOI: 10.4028/www.scientific.net/MSF.471-472.414.

10. Huang P., Li J., Sun J., Ge M. Milling force vibration analysis in high speed milling of Ti alloy using variable pitch angle mill. *International Journal of Advanced Manufacturing Technology*, 2012, vol. 58, pp. 153–160. DOI: 10.1007/s00170-011-3380-9.

11. Abele E., Fröhlich B. High speed milling of titanium alloys. *Advances in Production Engineering & Management*, 2008, vol. 3, pp. 131–140.

12. Da Silva R.B., Machado Á.R., Ezugwu E.O., Bonney J., Sales W.F. Tool life and wear mechanisms in high speed machining of Ti-6Al-4V alloy with PCD tools under various coolant pressures. *Journal of Materials Processing Technology*, 2013, vol. 213, pp. 1459–1464. DOI: 10.1016/j.jmatprotec.2013.03.008.

13. Wang Q., Chen X., An Q., Chen M., Guo H., He Y. Research on cutting performance and tool life improvement methods of titanium alloy ultra-high speed milling tools. *Journal of Manufacturing Processes*, 2024, vol. 131, pp. 38–51. DOI: 10.1016/j.jmapro.2024.09.018.

14. Ullah I., Akinlabi E.T., Songmene V. Thermo-metallo-mechanical based phase transformation modeling for high-speed milling of Ti-6Al-4V through stress-strain and temperature effects. *Journal of Materials Research and Technology*, 2024, vol. 30, pp. 894–909. DOI: 10.1016/j.jmrt.2024.03.096.

15. Raghavendra S., Sathyanarayanab P.S., Selvakumar S., Thangarasu V.S., Manjunatha K.N. High speed machining of titanium Ti6Al4V alloy components: study and optimisation of cutting parameters using RSM. *Advances in Materials and Processing Technologies*, 2020, vol. 8, pp. 277–290. DOI: 10.1080/2374068X.2020.1806684.

16. Abbas A.T., Sharma N., Anwar S., Hashmi F.H., Jamil M., Hegab H. Towards optimization of surface roughness and productivity aspects during high-speed machining of Ti-6Al-4V. *Materials*, 2019, vol. 12, p. 3749. DOI: 10.3390/ma12223749.

17. Gao Y., Wang G., Liu B. Chip formation characteristics in the machining of titanium alloys: A review. *International Journal of Machining and Machinability of Materials*, 2016, vol. 18, p. 155. DOI: 10.1504/IJMMM.2016.075467.

18. Jawaid A., Sharif S., Koksal S. Evaluation of wear mechanisms of coated carbide tools when face milling titanium alloy. *Journal of Materials Processing Technology*, 2000, vol. 99, pp. 266–274. DOI: 10.1016/S0924-0136(99)00438-0.

19. Zhang Y.P., Xu J.H., Geng G.S. Tool wear and surface integrity in high speed milling of a near alpha titanium alloy. *Materials Science Forum*, 2006, vol. 532–533, pp. 644–647. DOI: 10.4028/www.scientific.net/MSF.532-533.644.

20. Elmagrabi N., Che Haron C.H., Jaharah A.G., Shuaeib F.M. High speed milling of Ti-6Al-4V using coated carbide tools. *European Journal of Scientific Research*, 2008, vol. 22, pp. 153–160.

21. Kumar Khare S., Singh Phull G. Tool wear and surface roughness evaluation of mill insert tools in high-speed machining of Ti-6Al-4 V. *Materials Today: Proceedings*, 2023. DOI: 10.1016/j.matpr.2023.01.297.

22. Ginting A., Nouari M. Experimental and numerical studies on the performance of alloyed carbide tool in dry milling of aerospace material. *International Journal of Machine Tools and Manufacture*, 2006, vol. 46, pp. 758–768. DOI: 10.1016/j.ijmachtools.2005.07.032.

23. Denkena B., Biermann D. Cutting edge geometries. *CIRP Annals*, 2014, vol. 63, pp. 631–653. DOI: 10.1016/j.cirp.2014.05.009.

24. Denkena B., Koehler J., Rehe M. Influence of the honed cutting edge on tool wear and surface integrity in slot milling of 42CrMo4 ыteel. *Procedia CIRP*, 2012, vol. 1, pp. 190–195. DOI: 10.1016/j.procir.2012.04.033.

25. Jenkins R., Snyder R.L. *Introduction to X-ray powder diffractometry*. New York, Wiley, 1996. 403 p. ISBN 0-471-51339-3.

26. Stokes A.R., Wilson A.J.C. The diffraction of X-rays by distorted crystal aggregates. *Proceedings of the Physical Society*, 1944, vol. 56, pp. 174–181. DOI: 10.1088/0959-5309/56/3/303.

27. Zhang J., Kozlov V.N., Liu S. Influence of wear-resistant coating on the reliability of replaceable inserts in cutting steel. *IOP Conference Series: Materials Science and Engineering*, 2020, vol. 795, p. 012023. DOI: 10.1088/1757-899X/795/1/012023.

28. Kozlov V.N., Zhang J.Y., Guo Y.B., Sabavath S.K. Calculation of contact stresses during titanium alloy cutting. *Key Engineering Materials*, 2018, vol. 769, pp. 364–370. DOI: 10.4028/www.scientific.net/KEM.769.364.

29. Geng G.S. Xu J.H., Fu Y.C., Ge Y.F., Su C. Cutting temperature in high speed milling of a near alpha titanium alloy. *Key Engineering Materials*, 2006, vol. 315–316, pp. 145–149. DOI: 10.4028/www.scientific.net/KEM.315-316.145.

30. Pramanik A. Problems and solutions in machining of titanium alloys. *International Journal of Advanced Manufacturing Technology*, 2014, vol. 70, pp. 919–928. DOI: 10.1007/s00170-013-5326-x.

31. Liu H.G., Zhang J., Jiang Y., He Y., Xu X., Zhao W. Investigation on morphological evolution of chips for Ti6Al4V alloys with the increasing milling speed. *Procedia CIRP*, 2016, vol. 46, pp. 408–411. DOI: 10.1016/j.procir.2016.03.127.

32. Sun S., Brandt M., Dargusch M.S. Characteristics of cutting forces and chip formation in machining of titanium alloys. *International Journal of Machine Tools and Manufacture*, 2009, vol. 49, pp. 561–568. DOI: 10.1016/j.ijmachtools.2009.02.008.

33. Amin A.K.M.N., Ismail A.F., Nor Khairusshima M.K. Effectiveness of uncoated WC–Co and PCD inserts in end milling of titanium alloy – Ti-6Al-4V. *Journal of Materials Processing Technology*, 2007, vol. 192–193, pp. 147–158. DOI: 10.1016/j.jmatprotec.2007.04.095.

34. Chen Y., Chen T. Study on cutting performance in ultrasonic−assisted milling of titanium alloy with circular−arc milling cutters. *International Journal of Advanced Manufacturing Technology*, 2022, vol. 120, pp. 415–425. DOI: 10.1007/s00170-022-08818-9.

35. Shyha I., Gariani S., El-Sayed M.A., Huo D. Analysis of microstructure and chip formation when machining Ti-6Al-4V. *Metals*, 2018, vol. 8 (3), p. 185. DOI: 10.3390/met8030185.

36. Sun S. Observation and quantitative characterization of geometric and cyclical features associated with chip segmentation during machining of Ti6Al4V alloy. *Journal of Materials Processing Technology*, 2025, vol. 338, p. 118794. DOI: 10.1016/j.jmatprotec.2025.118794.

37. Kozlov V., Gerasimov A., Kim A. Distribution of contact loads over the flank-land of the cutter with a rounded cutting edge. *IOP Conference Series: Materials Science and Engineering*, 2016, vol. 124, p. 012173. DOI: 10.1088/1757-899X/124/1/012173.

38. Mesquita R.A. *Tool steels: Properties and performance*. Boca Raton, CRC Press, 2021. 257 p. ISBN 9780367782573.

39. Che-Haron C.H. Tool life and surface integrity in turning titanium alloy. *Journal of Materials Processing Technology*, 2001, vol. 118, pp. 231–237. DOI: 10.1016/S0924-0136(01)00926-8.

Conflicts of Interest

The authors declare no conflict of interest.